Cryogenic optical refrigeration

Denis V. Seletskiy[1,3], Markus P. Hehlen[2], Richard I. Epstein[1] and Mansoor Sheik-Bahae[1]

[1]Department of Physics and Astronomy, University of New Mexico, Albuquerque, New Mexico 87131, USA

[2]Los Alamos National Laboratory, Materials Science and Technology Division, Los Alamos, New Mexico 87545, USA

[3]Air Force Research Laboratory, Space Vehicles Directorate, Kirtland AFB, New Mexico 87117, USA (d.seletskiy@gmail.com)

Received November 9, 2011; revised February 9, 2012; accepted February 13, 2012; published March 22, 2012 (Doc. ID 157833)

We review the field of laser cooling of solids, focusing our attention on the recent advances in cryogenic cooling of an ytterbium-doped fluoride crystal (Yb^{3+}:$YLiF_4$). Recently, bulk cooling in this material to 155 K has been observed upon excitation near the lowest-energy (E4–E5) crystal-field resonance of Yb^{3+}. Furthermore, local cooling in the same material to a minimum achievable temperature of 110 K has been measured, in agreement with the predictions of the laser cooling model. This value is limited only by the current material purity. Advanced material synthesis approaches reviewed here would allow reaching temperatures approaching 80 K. Current results and projected improvements position optical refrigeration as the only viable all-solid-state cooling approach for cryogenic temperatures.

OCIS codes: 020.3320, 300.2530

Cryogenic optical refrigeration

Denis V. Seletskiy, Markus P. Hehlen, Richard I. Epstein and Mansoor Sheik-Bahae

1. Introduction

"Laser cooling" can be defined as a process by which a physical system cools upon interaction with laser light. In other words, laser light is used to directly lower the energy contained in a given internal degree of freedom of the system. One concept of laser cooling is perhaps best known for the case of Doppler cooling [1], which upon its demonstration resulted in the 1997 Nobel Prize in Physics [2]. Such cooling is based on inelastic interaction (Doppler shift) of a system of atoms, ions, or molecules [3] in a dilute gas phase with counterpropagating laser beams. Properly tuned laser light imposes a viscous drag ("optical molasses" [4]) on the moving constituents of the gas, slowing them down to velocities consistent with gas temperatures near $(10^{-6} - 1)$ K. In this process, energy contained in the translational degrees of freedom of the gas is lowered. Doppler cooling has enabled the observation of Bose–Einstein condensates that received the 2001 Nobel Prize in Physics [5].

At moderately high temperatures (~10–400 K), the thermal energy of the physical systems is contained mostly in the vibrational degrees of freedom. In 1929, Peter Pringsheim proposed the use of narrowband optical radiation to lower energy of these modes through fluorescence upconversion [6]. Lev Landau reconciled cooling matter with light with thermodynamics by considering the entropy of the radiation [7]. Laser-mediated cooling of vibrational degrees of freedom has been termed "optical refrigeration" or "laser cooling" of solids. The concept of cooling via fluorescence upconversion (optical refrigeration) has been verified in proof-of-principle demonstrations in gases [8], solids [9], and liquids [10]. In the case of solids, laser energy is initially deposited into the lowest-energy electronic states of a dopant ion in a solid. These states then thermalize with the environment by absorbing energy from the vibrational modes of the host and carry that energy out of the system through fluorescence radiation.

For recent reviews of the field of laser cooling of solids the reader is referred to Refs. [11–15]. In this paper, we review recent developments of laser cooling to cryogenic temperatures using the trivalent rare-earth ion ytterbium (Yb^{3+}) doped into a transparent crystalline host of yttrium lithium fluoride ($YLiF_4$), Yb:YLF. Following the Introduction, in Section 2 we review a rate-equation-based model of the laser cooling efficiency and its experimental verification in Subsection 2.3. Section 3 discusses thermal and optical design considerations for high-power bulk cooling

Figure 1

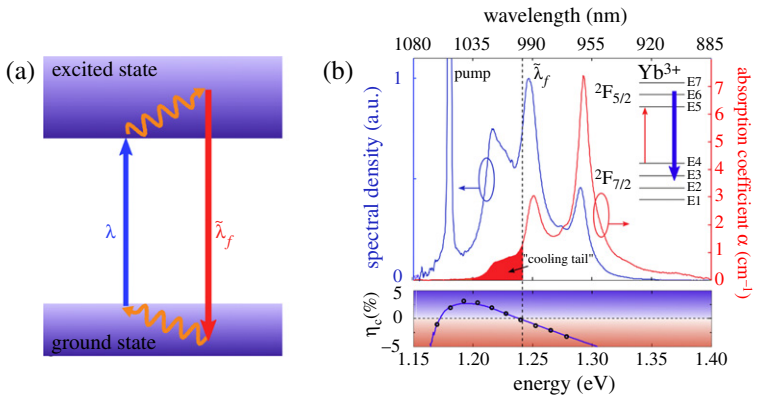

(a) Schematic energy diagram of a laser cooling cycle in a solid: an optical input at wavelength λ excites the lowest-energy electronic transition from a ground state to an excited state of an exemplary ion doped into a transparent host matrix. After thermalization via phonon absorption from the host (wavy arrows within manifolds), excitation relaxes radiatively with an mean emission wavelength $\tilde{\lambda}_f < \lambda$. (b) (adapted from [16]) Top, absorption (red) and emission (blue) spectra for an optical transition between $^2F_{7/2}$ and $^2F_{5/2}$ multiplet states of Yb^{3+}-doped $YLiF_4$ (Yb:YLF) at 300 K; excitation (labeled "pump") is below the mean emission wavelength $\tilde{\lambda}_f$, i.e., in the "cooling tail" (shaded) of the absorption curve. Bottom, data points (open circles) and fit of the cooling efficiency (η_c) spectrum of Yb:YLF. Cooling (η_c) occurs slightly below $\tilde{\lambda}_f$ and reverses sign at longer wavelengths because of heat-producing background absorption.

to cryogenic temperatures and focuses on the recent demonstration of cryogenic operation in Yb:YLF. In Section 4, we conclude by reviewing advanced material synthesis approaches that are necessary to enable laser cooling to temperatures approaching the boiling point of nitrogen.

Nearly thirty years before the invention of the laser, Pringsheim proposed cooling of solids through fluorescence upconversion by use of narrowband optical radiation [6]. Optical refrigeration or laser cooling of solids is based on anti-Stokes fluorescence. Consider an electronic transition in a dopant ion with a mean emission (fluorescence) wavelength of $\tilde{\lambda}_f$ [Fig. 1(a)]. Following resonant absorption in the long-wavelength (cooling) tail of such a transition ($\lambda > \tilde{\lambda}_f$), the generated low-energy electronic excitation undergoes ultrafast thermalization through inelastic scattering with the vibrational modes of the host lattice, thereby gaining energy in the process (i.e., phonon absorption). This additional energy is supplied by the lattice, which cools as a result of this interaction. Bulk cooling of the solid is possible if the decay of these electronic excited states is predominantly radiative. The idealized cooling efficiency (η_c) of such a process can be defined as [12]

$$\eta_c = \frac{h\tilde{\nu}_f - h\nu}{h\nu} = \frac{\lambda}{\tilde{\lambda}_f} - 1, \tag{1}$$

which is the ratio of the energy gained by inelastic scattering (phonon absorption) to the input energy, where $\nu = c/\lambda$. A positive η_c corresponds to cooling in this definition. As will be derived formally in Subsection 2.1, a realistic cooling efficiency has to address the possibility of heat-producing events such as nonradiative decay and absorption by impurities. These processes reduce the probability of conversion of an absorbed photon into an escaped fluorescence photon $p(\lambda)$, modifying Eq. (1) to

$$\eta_c = p(\lambda)\frac{\lambda}{\tilde{\lambda}_f} - 1. \tag{2}$$

$p(\lambda)$ is given as a product of external quantum efficiency (η_{ext}) and absorption efficiency [$\eta_{\text{abs}}(\lambda)$], defined in the following. The η_{ext} represents the probability with which a decay of a photoexcited dopant ion can produce an escaped fluorescence photon and is given by the ratio $\eta_e W_r/(\eta_e W_r + W_{nr})$, where W_r and W_{nr} are the radiative and nonradiative decay rates, respectively. The spontaneous emission is inhibited by the fluorescence escape efficiency η_e, which accounts for effects of total internal reflection trapping and reabsorption [17,18]. Similarly, the absorption efficiency $\eta_{\text{abs}}(\lambda)$ is the probability of a pump absorption leading to photoexcitation of a dopant ion, and it is given by the ratio $\alpha_r(\lambda)/(\alpha_r(\lambda)+\alpha_b)$, where $\alpha_r(\lambda)$ and α_b are the resonant (ion) and background absorption coefficients, respectively. As will be discussed in Section 4, background absorption in laser cooling materials is typically broadband and therefore can be treated as a constant within a given resonant absorption spectrum.

The net cooling condition ($\eta_c > 0$) restricts the joint probability to values $p(\lambda) > 1 - \Delta/\tilde{\lambda}_f$. For a practical excitation detuning $\Delta = \lambda - \tilde{\lambda}_f \sim hc/(k_B T)$, p has to be larger than 96% and 99% at 300 K and 77 K, respectively. Figure 1(b) depicts absorption and fluorescence spectra of a Yb:YLF crystal, along with the measured cooling efficiency spectrum. Even if the cooling condition is satisfied in the region where $\lambda < \tilde{\lambda}_f$, the sign of η_c is eventually reversed with further increase of the positive detuning owing to a decrease of $\eta_{\text{abs}}(\lambda)$. Thus, the key requirements for the laser cooling process are both a high-quantum-efficiency dopant transition and a high host purity.

The advantages of using high-quantum-efficiency atomic transitions for laser cooling of solids were recognized early on. In particular, Kastler [19] and Yatsiv [20] suggested that rare-earth-doped materials could be used for optical refrigeration. The high quantum efficiency of rare-earth ions is a result of the efficient screening of the 4*f* electron orbitals by 5*s* and 6*s* outer shells. This reduces electron–phonon coupling and suppresses nonradiative multiphonon relaxation of excited 4*f* electronic states. The screening of the 4*f* orbitals minimizes the Stokes shift of the emission associated with the parity-forbidden 4*f*–4*f* transitions, allowing states with relatively large absorption cross sections to be utilized for the laser cooling (anti-Stokes) process. The $(2J+1)$-degeneracy associated with the $^{2S+1}L_J$ multiplets of a 4*f* configuration is partially or completely lifted by the interaction with the crystal field of the host. In the case of Yb^{3+}, this results in a splitting of the $^2F_{7/2}$ and $^2F_{5/2}$ multiplets into 4 and 3 Stark levels, respectively (for point symmetries lower than cubic).

Following these considerations, Kushida and Geusic [21] reported reduced heating in a Nd^{3+}:YAG crystal when excited by a 1064-nm laser, which they attributed to cooling via anti-Stokes emission. The first demonstration of net laser cooling of a solid was accomplished in 1995 by Epstein and co-workers at Los Alamos National Laboratory using a highly pure ytterbium-doped fluorozirconate glass Yb^{3+}:ZBLANP [9]. Since then, optical refrigeration has been confirmed in a variety of glasses and crystals doped with Yb^{3+} (ZBLANP [9,22–25], ZBLAN [26–31], ZBLANI [32], CNBZn [33,34], BIG [28,35,36], $KGd(WO_4)_2$ [37], $KY(WO_4)_2$ [37], YAG [37,38], Y_2SiO_5 [38], KPb_2Cl_5 [33,39], BaY_2F_8 [40,41], YLF [42–44], ABCYS [45]), Tm^{3+} (ZBLAN [46,47], BYF [48]), and Er^{3+} (CNBZn [49], KPb_2Cl_5 [49,50]). The inverse dependence of the cooling efficiency η_c on the pump energy [Eq. (1)] has been verified in experiments with Tm^{3+} [47].

Because electronic states in rare-earth-doped solids are localized, their thermal population is governed by Boltzmann statistics. The thermal population of the excited Stark level [see Fig. 1(a)] of the pumped transition decreases with decreasing temperature, leading to a precipitous reduction of the absorption cross section and thus cooling efficiency at low temperatures. This effect limits the possibility of laser cooling of rare-earth-doped solids at temperatures below about 50 K. In principle this limit does not exist for laser cooling of semiconductors whose electrons and holes are indistinguishable and which thus obey Fermi–Dirac statistics. The feasibility of laser cooling in semiconductors has been extensively investigated both theoretically [17,51–61] and experimentally [61–69]; however, no net temperature reduction has been observed yet. This failure is due to stringent purity requirements, complications associated with inefficient light extraction from the high-refractive-index substrate ($\eta_e < 0.2$ for nearly index-matched dome [17,66]), and many-body effects such as a carrier-density-dependent quantum efficiency.

Many innovative applications of laser cooling have been proposed, including an all-solid-state optical cryocooler [26,70] and lasers with without internal heat generation [71,72]. Motivated by the former, one of the major ongoing directions in optical refrigeration research has been toward a demonstration of cryogenic temperatures. Research on laser cooling of Yb^{3+}:ZBLAN fluoride glass has culminated with the Los Alamos team demonstrating absolute temperatures of 208 K in 2005 [25]. This result was accomplished by maximizing pump light trapping in and minimizing thermal loads on a sample.

A significant breakthrough came with the realization that the cooling efficiency can be dramatically enhanced in rare-earth-doped crystalline hosts [16], compared with amorphous hosts of similar material purity [Fig. 2]. This is because the long-range order in a crystalline host leads to less inhomogeneous broadening of the crystal-field transitions in comparison with the glassy matrix. This preserves the peak absorption cross section at the Stark-level resonances and therefore, through a corresponding enhancement of the absorption efficiency η_{abs}, allows for cooling to much lower temperatures compared with glassy materials with the same purity. In addition, higher dopant concentrations are possible for stoichiometric crystal hosts. Using these

Figure 2

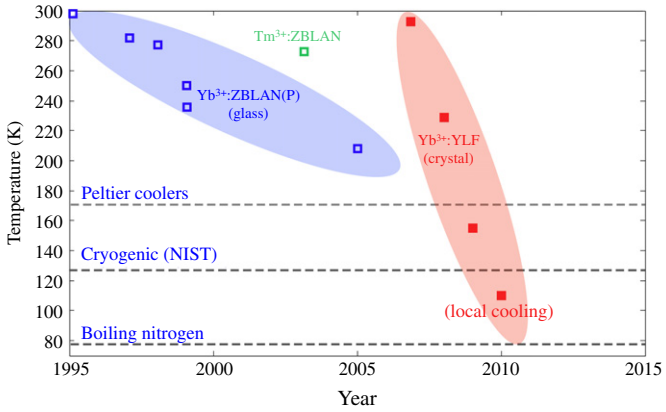

Timeline of the progress in optical refrigeration of bulk rare-earth-doped solids. A clear distinction between ytterbium-doped glasses (blue shaded region) and an ytterbium-doped YLF crystal (red) can be seen. Local cooling in the latter has been verified at 110 K, surpassing the NIST-defined cryogenic temperature of 123 K.

ideas, the University of New Mexico team cooled Yb:YLF crystals to an absolute temperature of 155 K [16] when pumping near the E4–E5 crystal-field transition ([73]; see Subsection 3.2). The lowest possible temperature in these experiments was limited by the pump laser that was used, which had relatively low power and an excitation wavelength that was detuned from the desired E4–E5 resonance. Despite these limitations, the demonstrated performance surpassed the lowest temperatures achievable by standard thermo-electric coolers and has positioned laser cooling of solids as the only current all-solid-state cryogenic refrigeration technology. Subsequently, laser cooling to 165 K of a semiconductor attached to a Yb:YLF crystal was accomplished, demonstrating successful cooling of a thermal load that mimicked an actual optoelectronic device [74]. As described in the next section, the laser cooling efficiency model predicts minimum temperatures of ~115 K when current-purity Yb:YLF samples are excited directly at the E4–E5 crystal-field resonance [16]. These predictions were verified using a noncontact pump–probe temperature measurement technique (Subsection 2.3), where local cooling to 110 K was observed [75]. Thus, laser cooling below the NIST-defined cryogenic point of 123 K (−150°C) is feasible. Cooling to absolute temperatures approaching 80 K can be achieved with a factor of ten improvement in the purity of Yb:YLF crystals [75] (see Section 4).

It is important to note recent progress in other novel laser cooling schemes. A process of collisional redistribution of radiation [76,77] was demonstrated to cool dense gases by 120 K, starting at ~500 K [78]. Spontaneous Brillouin scattering has been utilized to cool targeted vibrational modes of a microresonator [79]. Coherent processes invoking stimulated Raman scattering [80,81] and superradiance [82,83] were also proposed for laser cooling applications. Athermal lasers and amplifiers have been proposed, where the active medium is co-doped with rare-earth ions [84–87]. In contrast to cooling of the internal degrees

Figure 3

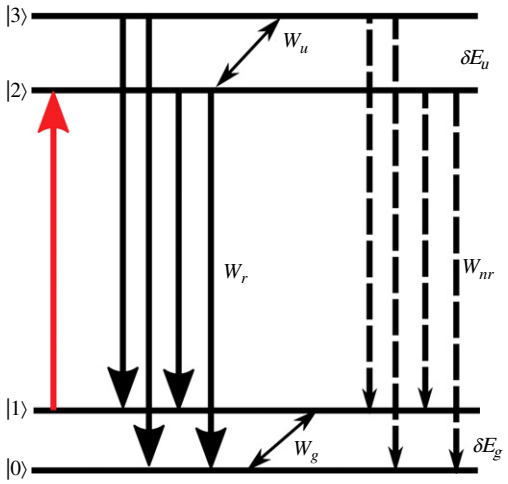

The four-level model consists of ground ($|0\rangle, |1\rangle$) and excited ($|2\rangle, |3\rangle$) state multiplets with respective energy separations $\delta E_{g,u}$ and intramultiplet electron–phonon interaction rates $w_{g,u}$. Inter-multiplet recombination occurs via radiative (W_r) or nonradiative (W_{nr}) decay channels, following the excitation of the lowest-energy transition ($|1\rangle$–$|2\rangle$, red arrow).

of freedom of a system, the interaction of a laser with macroscopic (Brownian) motion can be used to lower the kinetic energy of said system along a specific direction [88]. An optomechanical resonator was cooled to its corresponding quantum ground state by using this approach [89].

2. Principles of Solid-State Laser Cooling

In this section we review a rate-equation-based model of the laser cooling efficiency that builds on experimentally accessible macroscopic quantities. We point out that microscopic theories of the cooling cycle have also been developed [90–92], but they are beyond the scope of this review.

2.1. Four-level Model

Following Ref. [13], we consider a four-level system where closely-spaced $|0\rangle$ and $|1\rangle$ energy levels comprise a ground-state multiplet, and $|2\rangle$ and $|3\rangle$ refer to the closely-spaced levels of the excited-state multiplet [Fig. 3]. The incident laser of energy $h\nu = E_{21}(E_{ij} = E_i - E_j)$ excites the $|1\rangle \rightarrow |2\rangle$ transition. Inter-multiplet relaxation occurs by either radiative (W_r) or nonradiative (W_{nr}) decay. For simplicity, we take the rate constants to be identical for all possible inter-multiplet transitions. Relaxations within the ground and excited multiplets are accounted for by the respective electron–phonon interaction rate constants w_g and w_u, also taken to be the same in the current model. Thus, the population den-

sity in the four levels evolves according to the following rate equations:

$$\frac{dN_1}{dt} = -\frac{\sigma_{12} I}{h\nu}(N_1 - N_2) + \frac{R}{2}(N_2 + N_3) - w_g(N_1 - N_0 e^{-\delta E_g/k_B T}) \quad (3a)$$

$$\frac{dN_2}{dt} = \frac{\sigma_{12} I}{h\nu}(N_1 - N_2) - RN_2 + w_u(N_3 - N_2 e^{-\delta E_u/k_B T}) \quad (3b)$$

$$\frac{dN_3}{dt} = -RN_3 - w_u(N_3 - N_2 e^{-\delta E_u/k_B T}) \quad (3c)$$

$$N_{tot} = N_0 + N_1 + N_2 + N_3 = \text{const}, \quad (3d)$$

where σ_{12} is the absorption cross section of the $|1\rangle \rightarrow |2\rangle$ transition, δE_g and δE_u are the widths of the ground and excited state multiplets, $R = 2(W_r + W_{nr})$, and equal degeneracy of all levels is assumed. The total power density deposited into the system is given by the difference between input (absorption) and output (emission) contributions:

$$P_{\text{net}} = P_{\text{abs}} - P_{\text{rad}} = [\alpha(I) + \alpha_b]I - W_r[N_2(E_{20} + E_{21}) + N_3(E_{30} + E_{31})], \quad (4)$$

where $\alpha(I) = \sigma_{12}(N_1 - N_2)$ and α_b are the resonant and the background absorption coefficients, respectively, the latter arising from the possibility of absorption events on impurity ions that lead to heating [93]. Cooling occurs when $P_{\text{net}} < 0$ [Eq. (4)], i.e., when the radiated power density exceeds the absorbed power density. The cooling efficiency η_c, defined as a ratio of the negative net deposited power density to the absorbed power density ($\eta_c = -P_{\text{net}}/P_{\text{abs}}$), together with Eq. (4), a steady-state solution of Eq. (3), and homogeneous broadening yields

$$\eta_c = \eta_{\text{ext}}\eta_{\text{abs}}(\nu, I)\frac{\nu_f}{\nu} - 1, \quad (5)$$

where $\eta_{\text{ext}} = \eta_e W_r/(\eta_e W_r + W_{nr})$ is the external quantum efficiency, which equals the internal quantum efficiency for unity fluorescence extraction efficiency η_e. The $\eta_{\text{abs}}(\nu, I)$ term is the absorption efficiency (defined below). By the sign convention adopted here, $\eta_c > 0$ corresponds to cooling. The mean emitted energy $h\nu_f$ is given by

$$h\nu_f = E_{12} + \frac{\delta E_g}{2} + \frac{\delta E_u}{1 + (1 + R/w_u)e^{\delta E_u/k_B T}}. \quad (6)$$

The absorption efficiency term η_{abs} in Eq. (4) is defined as a ratio of the absorption by the $|1\rangle \rightarrow |2\rangle$ transition to the total absorption, which includes parasitic processes:

$$\eta_{\text{abs}} = \frac{\alpha(I)}{\alpha(I) + \alpha_b} = \left[1 + \frac{\alpha_b(1 + I/I_s)}{\alpha_0}\right]^{-1}, \quad (7)$$

where $I_s = h\nu/\sigma_{12} g(\nu)\tau_{21}$ is the saturation intensity of a homogeneously broadened transition with decay lifetime τ_{21}. The expected frequency dependence of the absorption cross section σ_{12} is contained in the normalized lineshape function $g(\nu)$, given by a Lorentzian profile of width $w_u = w_g$. Saturation of the background absorption process can be successfully ignored because of its small absorption cross section as compared with σ_{12}. The unsaturated resonant absorption α_0 in Eq. (6) for

$E_{12} \gg k_B T$ is given by

$$\alpha_0(\nu) = \frac{\sigma_{12} g(\nu) N_t}{1 + e^{\delta E_g / k_B T}}. \tag{8}$$

Despite its simplicity, the four-level model conveys the essential features of the laser cooling process. The model shows that the cooling efficiency [Eq. (5)] is implicitly temperature dependent through the unsaturated resonant absorption [Eq. (8)] and the mean luminescence energy [Eq. (6)]. The reduction of α_0 and the redshift of ν_f with decreasing temperature lead to a corresponding decrease in the cooling efficiency. This implies the existence of a wavelength-dependent minimum achievable temperature (MAT(λ)), which is set formally by the $P_{\text{rad}} = P_{\text{abs}}$ or $\eta_c = 0$ condition. For temperatures below the MAT, $\eta_c < 0$ corresponds to the regime where laser cooling is not possible. For a given mean emission redshift, the exact value of the MAT critically depends on the ratio $\alpha_b/\alpha(I)$ and hence on the purity of the material. Thus, to achieve the coldest possible temperatures, a minimal temperature dependence of α_0 and ν_f are desired for a given material (fixed α_b). The former condition is achieved in materials with a narrow ground-state multiplet ($\delta E_g < k_B T$), while the latter is satisfied when $R \ll w_u$, a condition that precludes a phonon "bottleneck" in the process of intra-multiplet thermalization [68,93,94].

Saturation of the resonant absorption $\alpha(I) = \alpha_0/(1 + I/I_s)$ leads to an intensity-dependent reduction of the cooling efficiency through a corresponding reduction of η_{abs}. This saturation is equivalent to an increase in the effective background absorption $\alpha_b(1 + I/I_s)$ and thus a corresponding increase in the MAT. The presence of saturation sets a practical limit for the maximum cooling power density P_{max} that can be extracted from a laser cooler. P_{max} can be estimated by using the definition of the cooling efficiency ($P_{\text{cool}} = \eta_c P_{\text{abs}}$) together with Eq. (8) considered for $I = I_s$:

$$P_{\text{max}} \approx \frac{k_B T}{2\tau_{21}} \frac{N_t}{1 + e^{\delta E_g / k_B T}}, \tag{9}$$

where pump energy detuning of $k_B T$ is assumed. As expected, the maximum cooling power density is proportional to the total ion concentration and reduces with temperature because of a reduction of the resonant absorption [Eq. (8)].

The simplicity of the four-level model is appealing because it is based on only five experimentally observable quantities ($\lambda = c/\nu$): $\alpha_0(\lambda, T)$, $\lambda_f(T)$, η_q, α_b, and I_s. This allows for concrete predictions of the cooling performance, in particular of the unique MAT of a given material system.

2.2. Prediction of Cooling Efficiency in Yb:YLF

We now present measurements of the cooling efficiency of the ytterbium-doped $YLiF_4$ fluoride crystals and compare the results to the predictions of the four-level laser cooling model. The material used in this study was a high-purity Czochralski-grown 5 mol% doped Yb:YLF crystal [94].

Figure 4

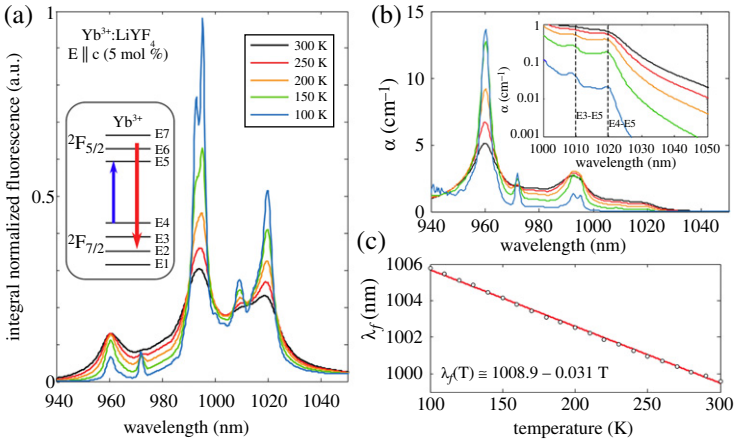

Temperature-dependent spectroscopic quantities of Yb:YLF (adapted from [95]). (a) Fluorescence spectra of a Yb:YLF crystal in $E\|c$ orientation normalized to the integrated value at 100 K; the inset shows crystal-field transitions between the Stark levels of the Yb^{3+} $^2F_{7/2}$ and $^2F_{5/2}$ multiplets. (b) Absorption spectra of a Yb:YLF (5 mol%) crystal with the same polarization and color coding as panel (a); the inset shows the long-wavelength absorption tail on a semilogarithmic scale, with the resonant features corresponding to the E3–E5 and E4–E5 crystal-field transitions. (c) Mean fluorescence wavelength $\lambda_f(T)$ along with an approximate linear fit in the temperature range of 100–300 K.

To obtain the laser cooling efficiency and in particular the MAT, four quantities need to be determined experimentally: $\alpha_0(\lambda, T)$, $\lambda_f(T)$, η_{ext}, and α_b; the pump intensity is taken to be far below saturation, $I \ll I_s$. The first two quantities are obtained from fluorescence spectra collected as a function of temperature [Fig. 4(a)] [96]. Reciprocity analysis [97] allows for the calculation of $\alpha_0(\lambda, T)$ [Fig. 4(b)] from the polarized ($E\|c$) fluorescence spectra [95]. The first moment of the angularly-averaged unpolarized fluorescence lineshape function [Fig. 4(a)] is used for the calculation of $\lambda_f(T)$ [Fig. 4(c)], where reabsorption is taken into account.

A separate measurement of the sample temperature change as a function of pump laser wavelength [Fig. 1(b)] is used to obtain $\eta_{\text{ext}} = 0.995 \pm 0.001$ and $\alpha_b = (4.0 \pm 0.2) \times 10^{-4}$ cm^{-1} at room temperature [96]. To proceed, we make the reasonable assumptions that both η_{ext} [98] and α_b are temperature independent [93]. We will revisit the validity of these assumptions in the next section.

Figure 5(b) depicts the cooling efficiency of Yb:YLF calculated by using Eq. (4) under the aforementioned approximations. The blue region corresponds to the "cooling window" where $\eta_c > 0$, while heating occurs in the red region where $\eta_c < 0$. The transition line separating the cooling and heating regions corresponds to the spectrum of the minimum achievable temperature, i.e., MAT(λ). The MAT(λ) spectrum is formally defined by the condition of $\eta_c(\lambda, T) = 0$. The lowest temperature in the MAT(λ) is termed "global-MAT" or MAT_g and occurs at λ_{opt}, for which $\partial(\text{MAT}(\lambda))/\partial\lambda|_{\lambda=\lambda_{\text{opt}}} = 0$. The cooling window narrows with decreasing temperature, being constrained by the mean luminescence redshift at

Figure 5

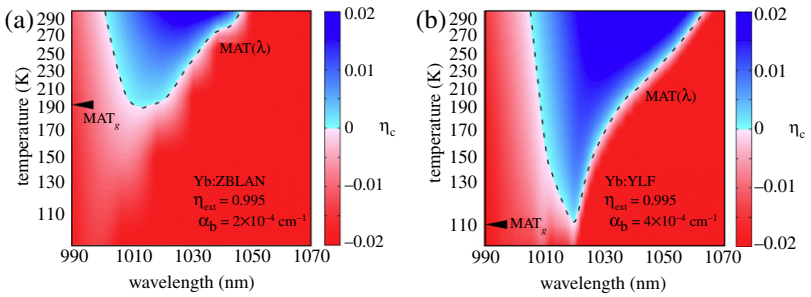

Comparison of cooling efficiencies in a glass and a crystal host (adapted from [95]): Contour plots of cooling efficiency $\eta_c(\lambda, T)$ for (a) Yb:ZBLAN and (b) Yb:YLF. The black dashed lines separating cooling (blue) and heating (red) regions correspond to the spectra of minimum achievable temperature, labeled MAT(λ). The effect of large inhomogeneous broadening in the glass host is evident from a lowest MAT (MAT_g) in Yb:ZBLAN of ∼190 K (at ∼1015 nm), compared with a MAT_g of ∼115 K (at 1020 nm) in Yb:YLF for otherwise similar parameters of η_{ext} and α_b.

short wavelengths and increasing $\alpha_b/\alpha(T)$ ratio at long wavelengths. This narrowing terminates at a single point that corresponds to MAT_g. The MAT_g for the given Yb:YLF sample is predicted to be ∼115 K at $\lambda_{opt} \sim 1020$ nm, corresponding to the wavelength of the E4–E5 crystal-field transition in Yb^{3+}. Figure 5(a) shows a similar analysis of the cooling efficiency in Yb:ZBLAN based on data obtained from earlier studies [99]. Both materials have similar quantum efficiency and background absorption; however a considerably higher MAT_g of 190 K is predicted for the glass host [95]. Previous results of cooling of Yb:ZBLAN at 1026 nm [25] are consistent with this estimate. Compared with the glass host, the crystal host achieves a lower MAT_g because of (i) smaller inhomogeneous broadening and (ii) a higher rare-earth ion concentration, both giving a larger peak absorption cross section of the E4–E5 transition.

To estimate the effect of saturation, Fig. 6(a) shows the MAT_g for a 5% Yb:YLF crystal as a function of an "effective background absorption" term $\alpha_b(1 + I/I_s)$. For unsaturated conditions, $\alpha_b = 4 \times 10^{-4}$ cm^{-1} corresponds to the $MAT_g \sim 115$ K which degrades with the excitation approaching saturation intensity. For example, $I = I_s$ would increase the MAT_g to ∼130 K. For practical considerations, where high cooling power densities are desired, a saturation-limited MAT has to be taken into an account. Figure 6(b) plots the maximum cooling power density, as calculated from the model [Eq. (9)] under $I = I_s$ excitation and for $\delta E_g \sim 60$ meV [100]. A MAT_g of ∼130 K with 3 W/m^3 is predicted to be possible for current-generation cryocoolers. We also note that an unsaturated MAT_g of ∼85 K is predicted for $\alpha_b = 4 \times 10^{-5}$ cm^{-1} [Fig. 6(a)]. Optical refrigeration to near the boiling point of nitrogen and colder should therefore be possible with the development of advanced material synthesis methods [Section 4].

Figure 6

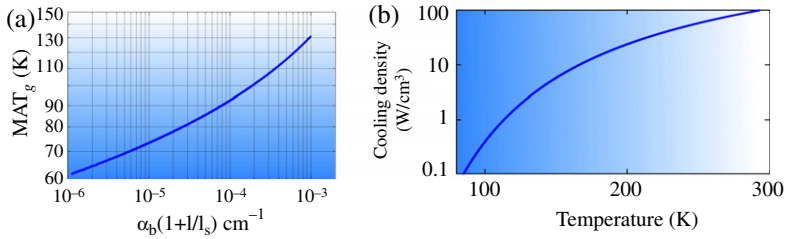

(a) Model prediction of the global minimum achievable temperature $\mathrm{MAT}_g = \mathrm{MAT}(1020\ \mathrm{nm})$ as a function of an effective background absorption in Yb:YLF (5 mol%, $E\|c$, $\eta_{\mathrm{ext}} = 0.995$). (b) Model prediction of the maximum cooling density that can be extracted from this material [Eq. (9)].

Figure 7

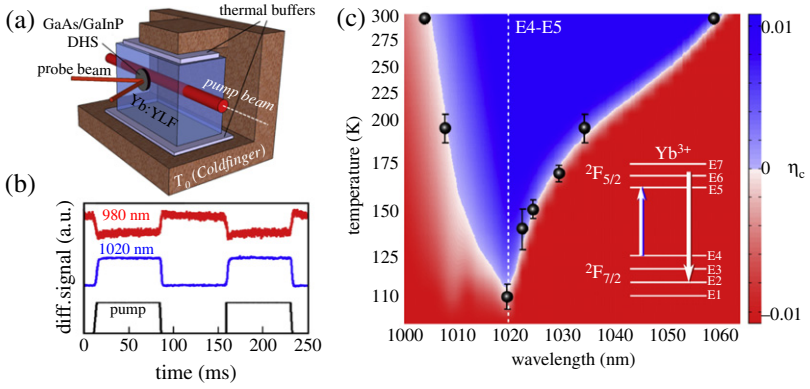

Experimental verification of the laser cooling model (adapted from [96]). (a) Schematic of the experimental arrangement: the Yb:YLF crystal is clamped by the cold-finger arrangement that is held at T_0; the local temperature change due to the pump beam is detected via luminescence from a GaAs/InGaP double heterostructure, excited in turn by a probe laser. Thermal buffers serve to maximize the local signal, while maintaining the Yb:YLF temperature near the T_0 setpoint. (b) Normalized and vertically shifted time traces of the spectral derivative signals, showing a distinct phase reversal between the heating (980 nm) and cooling (1020 nm) excitations at room temperature. (c) Comparison of the contour plot of the calculated cooling efficiency with the measurement (circles) of the minimum achievable temperature spectrum [MAT(λ)]; local cooling to a MAT of 110 ± 5 K at ∼1020 nm is demonstrated; the inset shows the energy-level diagram of Yb^{3+}(not to scale).

2.3. Experimental Verification of the Model

Local, transient laser cooling experiments were carried out to measure MAT(λ). For this, the overall temperature of the sample T_0 was adjusted in a cryostat [Fig. 7(a)]. The local temperature measurement probes the pump-induced temperature dynamics $T(t) = T_0 + \Delta T(t)$ within a small spatio-temporal (i.e., local) window defined by the excitation

beam and geometry-dependent thermal transport [75,101,102]. For a fixed excitation wavelength, T_0 was varied until the local temperature deviation ΔT changed sign from cooling to heating [Fig. 7(b)]. The T_0 at which this occurred corresponded to the MAT at that given wavelength.

The measurement of the MAT(λ) relied on a fast and highly sensitive thermometric technique: two-band differential spectral metrology (2B-DSM), which can rapidly measure temperature changes as small as 0.25 mK in semiconductors [75] and ~6 mK in glasses [103,104]. The measured MAT spectrum is shown in Fig. 7(c) and is in excellent agreement with the theoretically predicted values. In particular, the model prediction of a MAT_g of 115 K is in excellent agreement with the measured value of 110 $\pm$ 5 K. These measurements demonstrate the optical refrigeration potential of current-generation materials to cool below the NIST-defined cryogenic temperature of 123 K. The observed agreement in the cooling efficiency validates the laser cooling model and its assumptions, such as the temperature independence of quantum efficiency and background absorption.

3. Bulk Cooling

3.1. Thermal Load Optimization

The prospect of an all-solid-state cryocooler is the primary driver for laser cooling research to strive for the lowest possible temperature. To approach cooling temperatures near MAT, several important experimental considerations have to be addressed. These considerations are illustrated by the equation for temperature evolution, which follows from energy conservation [26]:

$$C\frac{dT}{dt} = \sum_i P_i = -P_{\mathrm{cool}}(\lambda, T) + P_{\mathrm{load}}(T), \tag{10}$$

where C is the heat capacity of the cooling sample, and P_{cool} and P_{load} are the cooling power load and environment heat load, respectively. To optimize cooling, P_{cool} and P_{load} terms need to be maximized and minimized, respectively.

The heat load term P_{load} is the sum of convective, conductive, and radiative heat loads. The first two respective contributions are lowered by carrying out the experiment in a vacuum chamber and by minimizing the contract area between the sample and its supports. Detailed modeling has shown that under these conditions the radiative or blackbody load is indeed the dominant contribution, and it is expressed as [26,105]

$$P_{bb} = \frac{\sigma \varepsilon_s A_s}{1+\chi}\left(T_c^4 - T^4\right), \tag{11}$$

where σ is the Stefan–Boltzmann constant (=5.67×10^{-8} $\mathrm{W/m^2/K^4}$), T_c is the environment (chamber) temperature, and $\chi = (1-\varepsilon_c)\varepsilon_s A_s/\varepsilon_c A_c$ with A_j and ε_j ($j = s, c$) representing the surface areas and thermal emissivities of the chamber and sample, respectively. Minimization of P_{bb} requires

maximization of χ, which is accomplished for small ε_c and A_c as well as $A_s/A_c \rightarrow 1$. These conditions are satisfied by making a tight-fitting "clamshell" chamber around the laser cooling crystal and lining it with a low-emissivity coating ($\varepsilon_c \sim 0.05$) [25].

The cooling power is given as a product of the cooling efficiency [Eq. (4)] and absorbed power (P_{abs}), i.e., $P_{\text{cool}} = \eta_c(\lambda, T)P_{\text{abs}}(\lambda, T)$. In Yb:YLF, the cooling efficiency is maximized for $\lambda_{\text{opt}} = 1020$ nm, corresponding to the E4–E5 crystal-field resonance. Maximization of P_{abs} is equivalent to maximization of the number of round trips N that the excitation at a fixed input power P_0 completes through the cooler. The effective interaction length NL can be increased by means of a nonresonant cavity, where the sample is placed between two dielectric mirrors with pump light admitted through a small entrance hole in the input mirror [25,47]. The mirrors can either form an external cavity or be deposited directly onto the sample. For the latter case it has been shown that residual absorption in dielectric mirror coatings can diminish laser cooling performance. Another approach is to couple pump light into totally internally reflected (trapped) modes of a laser cooling medium. Yet another approach uses a resonant cavity to interferometrically couple coherent excitation to cavity modes and an intracavity absorber. It has been known for some time [101–103] that absorption efficiencies approaching unity can be achieved for an arbitrary absorbance (αL) inside a resonator, provided that the reflectivity of the input coupling mirror (R_{ic}) satisfies the optical impedance matching condition (OIM). The OIM or "critical coupling" condition constrains the input-coupler reflectivity to $R_{ic} = \exp(-2\alpha L)$, when the back mirror reflectivity is assumed to be unity. Recently, the OIM condition for the intracavity absorber has been interpreted to be analogous to a "time-reversed" laser [104]. A true thermodynamic analogy of a laser running in reverse, however, requires a cavity with a "negative gain" that absorbs all of the input light, *cooling* the intracavity element in the process. Thus, intracavity optical refrigeration can indeed be thought of as the analog of a laser running in reverse!

Intracavity enhancement has been applied to Yb:ZBLAN, and an enhancement of the on-resonance absorption by a factor of 20 [Fig. 8(b)] compared with the single-pass value of αL was observed [31]; 93% of the theoretically predicted absorption was obtained at the cavity resonance [Fig. 8(a)]. The University of New Mexico team cooled Yb:ZBLAN by 3 K for an input power of 1 W at 1030 nm with this setup [31] and under conditions of minimized heat load. Likewise, they reported cooling of Yb:YLF by 69 K with 15 W of excitation at the same wavelength [43]. These experiments provided a first demonstration of a "laser running in reverse." Greater cooling was not obtained because of the challenges of cavity stabilization and the longitudinal mode instability of the high-power pump laser.

A solution to these challenges is to combine the cavities, i.e., to place the absorber inside the laser resonator. This eliminates the problems associated with the cavity-length stabilization and modal instability of the oscillator and allows for maximum absorption, provided the OIM condition is satisfied. Laser cooling of Yb:ZBLAN by 9 K has been achieved by using this concept [30], and a temperature drop of ~20 K was obtained in Yb:YLF when the crystal was placed inside of a VECSEL [106]. This is a promising approach to next-generation

Figure 8

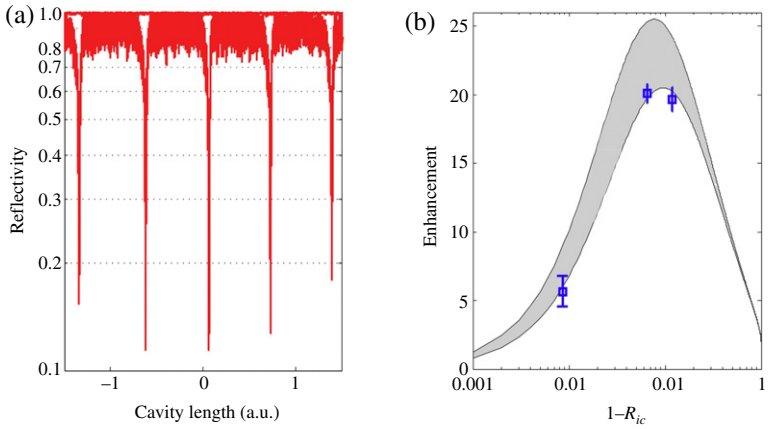

Cavity-enhanced resonant absorption (adapted from [31]). (a) The reflectivity of the cavity is shown as a function of cavity length. For a high-reflectivity back mirror, the cavity reflectivity $R = 1-A$, where A is the absorption. On resonance, R 11% corresponds to ~89% absorption, which is 93% of the ideal absorption as predicted from the analysis. (b) On-resonance enhancement (cavity absorption normalized to the single-pass absorption) is plotted for various values of input coupler reflectivity R_{ic} and compares favorably with the theory (OIM condition) for the given uncertainty (shaded gray area) in the αL value.

cryogenic optical refrigerators; however, as outlined in Subsection 3.3, the practical challenges of further heat load minimization, thermal link, and device miniaturization still remain to be demonstrated.

3.2. Cryogenic Cooling in Yb:YLF

The most successful approach to date for achieving coldest temperatures uses nonresonant cavities for maximizing the absorbed laser power [16,24–26,47]. The lowest absolute temperature of 155 K for bulk laser cooling reported to date used a 5 mol% Yb:YLF crystal pumped at 1023 nm so as to utilize the cooling efficiency enhancement near the E4–E5 crystal-field resonance [Subsection 2.2]. Experimental conditions ensured that the intensity was below the saturation intensity of a 5% Yb:YLF crystal [94]. The absorbed power was maximized by spatial mode matching of a high-power pump laser to a nonresonant cavity in which a Brewster-cut Yb:YLF crystal was placed [Fig. 9(a)]. Heat load minimization techniques were applied [Subsection 3.1], and the temperature was measured in a noncontact arrangement by monitoring spectrally resolved changes of the luminescence lineshape function [16,22,69,107], as shown in Fig. 9(b). To demonstrate the wavelength dependence of the cooling efficiency [Fig. 5(b)], cooling experiments were carried out for various wavelength and pump power conditions. The steady-state temperature was plotted versus the absorbed power [Fig. 9(c)]. These results clearly show a substantial enhancement of the cooling efficiency when the excitation wavelength approaches the E4–E5 crystal-field resonance at 1020 nm. The calculated steady-state temperature [calculated by equating cooling power to the

Figure 9

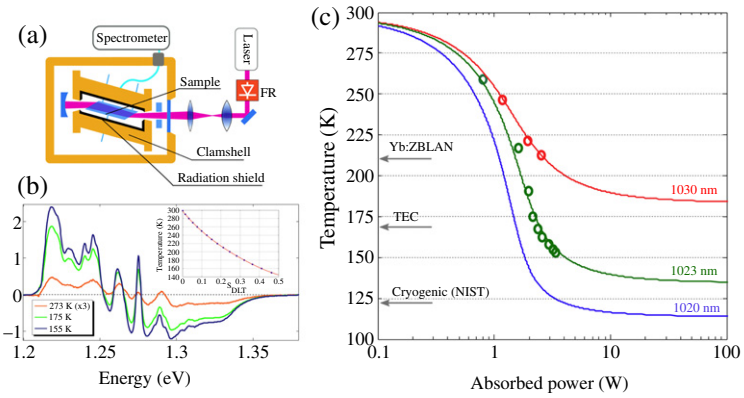

Cryogenic operation (adapted from [16]). (a) Schematic of the experimental setup where isolated (via a Faraday rotator, FR) and mode-matched pump light is trapped in a nonresonant cavity formed around the Yb:YLF sample inside of a clamshell. A spectrometer is used to measure the temperature of the sample by using a DLT method by extracting the temperature from normalized and reference-subtracted differential luminescence spectra, panel (b). The measured steady-state temperature (open circles) is plotted versus absorbed power and excitation wavelength along with the model fits (see text for details).

blackbody load in Eq. (11) and ignoring saturation] versus the absorbed power yields good agreement with the theory. This agreement not only validates the laser cooling model, but also independently confirms that the radiative load is the dominant load on the sample. We note that for high absorbed powers and unsaturated pumping, the calculated curves asymptote at the minimum achievable temperature for the given wavelength. The limited tuning of the Yb:YAG pump laser used for this study did not allow for high-power cooling at the exact E4–E5 resonance wavelength, but a calculation predicts that under similar experimental conditions, cooling to ~115 K is possible for absorbed powers of >4 W while on resonance [Fig. 9(c)].

The MAT of 115 K is an intrinsic limitation of the material purity of the current generation Yb:YLF crystals. As is shown in Subsection 2.2, an order of magnitude reduction of the background absorption coefficient in laser cooling crystals is projected to lower the MAT to near the nitrogen boiling point. The lower resonant absorption coefficient at liquid nitrogen temperatures renders multipass absorption enhancement schemes less practical because of the rising number of required round trips and associated increased mirror losses [108]. Thus, the future of cryogenic optical refrigeration relies on research in material synthesis together with optical engineering of intra-laser-cavity cooling approaches.

3.3. Device Considerations

The optical cryocooler offers several key advantages, including compactness, no vibrations (no moving parts or fluids), and high reliability.

Figure 10

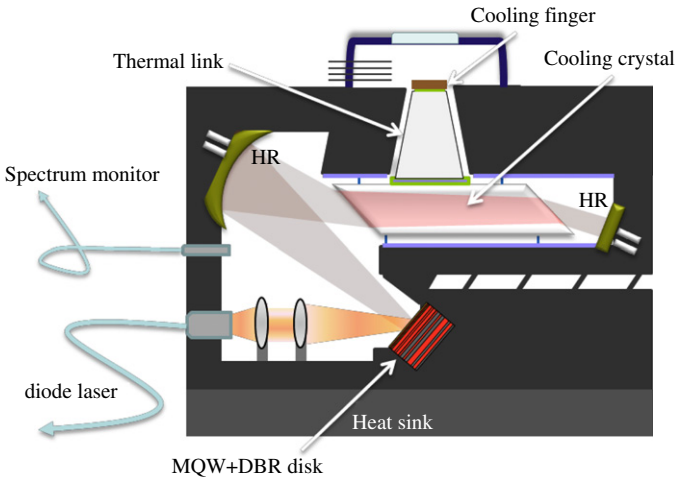

Illustration of a prototype all-solid-state optical refrigerator. A diode-pumped semiconductor laser cavity consisting of (i) multiple quantum-well (MQW) gain regions and an attached distributed Bragg reflector (DBR), (ii) cooling crystal, and (iii) high reflectivity (HR) end mirror. The cooling power from the crystal to the payload is transferred through a thermal link. A spectrum monitor optically measures the temperature of the cooling crystal.

Space-borne infrared sensors are likely to be the first beneficiaries, because imaging systems on space platforms are extremely sensitive to vibrations. Fundamentally, the size of the cryocooler is limited by only $\tilde{\lambda}_f^3$, which is the mode volume of a microscopically sized laser. The possibility of a microscale cooler is intriguing for basic science research as well as for local cooling of microelectronics. A study by Ball Aerospace Corporation showed that rare-earth-based optical refrigeration can outperform conventional thermoelectric and mechanical coolers for low-power, space-borne operations in the 80–170 K temperature range [109]. Current-generation Yb:YLF materials are pure enough to allow for demonstration of temperatures at or below the NIST-defined cryogenic barrier (123 K). Figure 10 illustrates a conceptual device that combines several ideas of performance optimization, as discussed above.

In particular, the absorption efficiency is enhanced by placing the impedance-matched cooling element inside a compact laser cavity [Subsection 3.2]. The use of high-efficiency pump diode lasers for VECSELs (or similar lasers) should further enhance the overall wall-plug efficiency of the cryocooler. Furthermore, the cooling efficiency can be maximized to approach the Carnot limit with the use of photovoltaic elements that recycle the waste photons [13]. The thermal link between the cooling element and the payload is one of the outstanding challenges for the laser cooler device. A successful thermal link design should incorporate properties of an efficient photon blockade (to prevent radiative heating of the load) in addition to possessing high thermal conductivity (to effectively remove heat from the load). Proposed [110] approaches for thermal link designs are yet to be demonstrated. With all of these technological improvements and ultrapure laser cooling

Figure 11

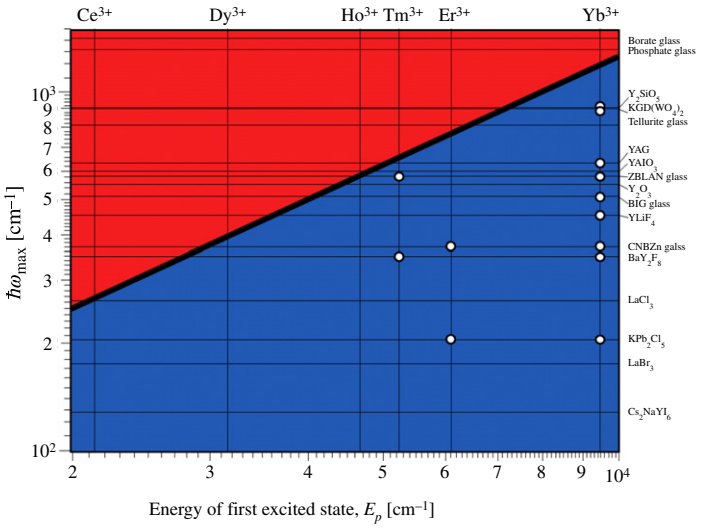

Combinations of active ions and host materials for optical refrigeration. Combinations for which the energy of the highest-energy optical phonon, $\hbar\omega_{\max}$, is less than $E_p/8$ (blue area) are expected to achieve >90% of the ideal cooling efficiency [Eq. (1)]. Materials in which laser cooling has been experimentally observed are indicated by the open circles [111].

materials, there are few barriers remaining for the realization of compact, high-efficiency all-solid-state cryocoolers.

4. Material Synthesis: Toward Sub-100 K Optical Refrigerators

The synthesis of materials for solid-state optical refrigerators is concerned mainly with maximizing the internal photon quantum efficiency in rare-earth-doped systems. Besides the desired radiative decay, the excited state can also relax by several unfavorable nonradiative decay mechanisms. These convert the electronic excitation into vibrational energy, heating up the lattice. The objective is to create a material with minimal nonradiative relaxation compared with its radiative relaxation.

A first consideration is the choice of the rare-earth ion and host material. The intrinsic nonradiative decay that occurs from the interaction of the rare-earth ion with the vibrational modes of the host itself has to be minimized. This is achieved by selecting a host material with a maximum optical phonon energy, $\hbar\omega_{\max}$, that is significantly smaller than the energy of the first excited electronic state of the rare-earth ion, E_p [111]. For many rare-earth ion excited states, the multiphonon relaxation rate becomes negligible compared with the radiative relaxation rate (i.e., the respective intrinsic quantum yield approaches unity) if $E_p/\hbar\omega_{\max} > 8$ [112]. In the case of Yb^{3+}, the $^2F_{5/2}$–$^2F_{7/2}$ energy gap of $E_p \approx 9500\ \text{cm}^{-1}$ therefore sets an upper limit of $\hbar\omega_{\max} \approx 1200\ \text{cm}^{-1}$. As shown in Fig. 11, this excludes most oxide glasses as host materials and narrows the set of practical hosts to oxide crystals (e.g., YAG, $YAlO_3$, Y_2O_3, $YSiO_5$),

fluoride glasses (e.g., ZBLAN, BIG), and fluoride crystals (e.g., $YLiF_4$, BaY_2F_8). For Yb^{3+}-doped fluoride crystals in particular, $E_p/\hbar\omega_{max} \approx 20$, which essentially eliminates nonradiative decay via interaction with host phonons [113]. Therefore, the even lower phonon energies of bromides, chlorides, and iodides ($\hbar\omega_{max} < 280$ cm^{-1} [112]) do not offer any further advantage for Yb^{3+}-based laser cooling materials, and the additional complexity associated with the extreme hygroscopicity, which is common in the heavy halides, can be avoided. The energy of the first excited state in Er^{3+}, Tr^{3+}, Ho^{3+}, or Dy^{3+} is smaller than that of Yb^{3+}, and these ions therefore offer a theoretically higher cooling efficiency than Yb^{3+} [see Eq. (1)]. The lower E_p, however, will require a lower $\hbar\omega_{max}$, and future laser cooling with Ho^{3+} or Dy^{3+} in particular will likely be possible only with chloride or bromide hosts.

We now turn to mitigating nonradiative decay that is introduced by impurities. A first class of impurities comprises molecules with high-energy vibrational modes such as the ubiquitous H_2O and OH^- but also complex anions such as NH_4^+. The excited state of a rare-earth ion in proximity to such a "vibrational impurity" will decay nonradiatively by coupling to a high-energy vibrational mode. For Yb^{3+} in proximity of an OH^- ion, which has a 3440 cm^{-1} stretching mode [114,115], the 9500 cm^{-1} energy gap of Yb^{3+} can be bridged by <3 vibrational quanta, making nonradiative relaxation of the Yb^{3+} $^2F_{5/2}$ excited state the dominant relaxation process. The need to maximize the resonant absorption coefficient α_0 necessitates rare-earth doping concentrations of typically >1 mol%, for which energy migration among the rare-earth ions becomes efficient. In such a scenario, Yb^{3+}-OH^- centers act as efficient nonradiative "traps" for excitation energy that can significantly degrade the overall laser cooling performance even at low concentrations [93]. Vibrational impurities can be minimized in the synthesis process. In the case of fluorides, the binary fluoride starting materials (e.g., YF_3, LiF, and YbF_3 for $YLiF_4$:Yb^{3+}) can be first individually treated in hot HF gas to reduce residual H_2O and OH^- impurities, and the subsequent preparation of a crystal or glass proceeds under inert atmosphere such as ultrahigh-purity argon [116–118].

A second class of impurities comprises trace metal ions having optical absorptions that are in resonance with the pump–emission wavelength of the rare-earth ion. Such impurities introduce two types of nonradiative decay (see Fig. 12): (1) pump laser energy absorbed directly by these ions manifests as background absorption [α_b, Eq. (6)] and generally decays nonradiatively; and (2) these ions can act as acceptors in a nonradiative energy transfer from the rare-earth ion and act, even at low concentrations, as efficient "traps" that can be reached via energy migration among the rare-earth ions. While many metal ions could, in principle, act as detrimental impurities, there is a smaller set of metals that are ubiquitous in commercial starting materials. The metals of concern include Fe, Ti, Mn, V, Cr, Ni, Cu, and Co. As shown in Fig. 12, the 2+ oxidation state of these transition metals, in particular, tends to have strong undesired absorptions in the near-infrared spectral region (4000–12000 cm^{-1}), where the laser cooling transitions of Yb^{3+}, Er^{3+}, Tm^{3+}, and Ho^{3+} occur, while the absorption bands associated with other oxidation states tend to be at higher energies. For example, Fe^{2+} has a

Figure 12

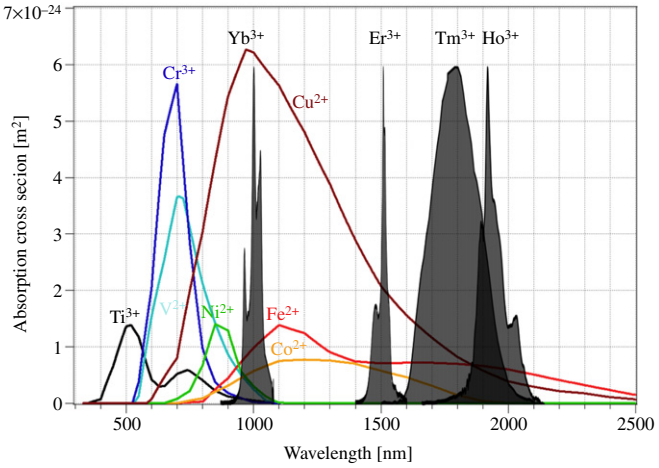

Absorption cross sections for various transition-metal ions in ZBLAN glass at room temperature (colored traces, adapted from [128]). The shaded areas show the luminescence spectra of Yb^{3+}:$YLiF_4$ [16], Er^{3+}:SiO_2, Tm^{3+}:ZBLAN [105], and Ho^{3+}:$Ba_2NaNb_2O_{15}$ [130]. Spectral overlap between a rare-earth luminescence and a transition-metal absorption indicates the possibility of quenching via nonradiative energy transfer. Transition-metal ions with 2+ oxidation states are particularly problematic in this respect.

$^5T_2 \rightarrow {}^5E$ absorption band around 10000 cm^{-1} in $RbFeF_3$ and $KFeF_3$, while the $^6A_{1g} \rightarrow {}^4T_{1g}, {}^4T_{2g}, {}^4A_{1g}, {}^4E_g$ absorption bands of Fe^{3+} in FeF_3 and $Li_3Na_3Fe_2F_{12}$ are all at >14000 cm^{-1} [119]. Similarly, Cr^{2+} has several broad absorptions in the 4000–14000 cm^{-1} region in CdF_2 [120], while the $^4A_2 \rightarrow {}^4T_2$ absorptions of Cr^{3+} in oxides and fluorides are all at >12000 cm^{-1} [121–125]. The V^{2+} $^4A_2 \rightarrow {}^4T_2, {}^4T_1$ absorptions in $CsCaF_3$ and $KMgF_3$ occur around 8000–12000 cm^{-1} [124,126], Ni^{2+} has broad absorptions in the 4000–14000 cm^{-1} range in CdF_2 [120] and fluoride glass [127], and the $^4T_2, {}^4T_1$ absorptions of Co^{2+} occur between 3000 and 25000 cm^{-1} in CdF_2 [120], $KMgF_3$ [121], and ZnF_2 [121]. Cu^{2+} absorbs strongly in the 5000–17000 cm^{-1} range in fluorides [128], while the Cu^+ absorptions in $RbMgF_3$ are all at >25000 cm^{-1} [129].

Calculations indicate that the concentration of transition-metal impurities has to be no greater than 10–100 ppb (parts in 10^9) to not substantially degrade a laser cooling material such as Yb^{3+}:ZBLAN [93]. Reducing transition-metal impurities to such low levels has two distinct aspects. First, typical commercial fluoride starting materials have transition-metal impurities at the parts per million (parts in 10^6) level. Such materials are not sufficiently pure for use in a direct synthesis of a laser cooling material, and purification of the staring material is required. The chemical inertness of the binary fluorides, however, prevents the use of standard purification methods (e.g., sublimation, recrystallization, ion exchange, solvent extraction) and makes their purification difficult. One approach to creating pure laser cooling materials [131] begins with the respective oxides, carbonates, chlorides, or metals that can be dissolved in acids, purified by solvent extraction, precipitated as

fluorides with hydrofluoric acid, and finally converted to high-purity binary fluorides by drying in hot HF gas. This comprehensive process has been demonstrated for each of the ZrF_4, BaF_2, LaF_3, AlF_3, NaF, InF_3, and YbF_3 precursors of the Yb^{3+}:ZBLANI laser cooling glass [131]. In this study, an ~725 fold reduction in transition-metal impurities over the initial commercial purity was measured, achieving a final residual transition-metal concentration of ~100 ppb that was suited for the subsequent synthesis of a high-performance laser cooling material. Second, the growth of a laser cooling crystal represents in itself a purification process. Controlled crystal growth tends to exclude ions that are not part of the ideal crystal lattice. In addition, the growth of a crystal tends to prefer specific oxidation states of the impurities that are incorporated. During the crystal growth of $YLiF_4$, for example, impurities of oxidation state 1+ (Li^+ site) and 3+ (Y^{3+} site) are expected to be incorporated more likely than impurities with 2+ and 4+ oxidation states. Incorporation of the latter requires formation of charge-compensated sites which may energetically be less favorable. As shown in Fig. 12, the 2+ transition metals are particularly detrimental with regards to acting as acceptors in an energy transfer from Yb^{3+}, Er^{3+}, Tm^{3+}, or Ho^{3+}. Their potential suppression during the crystal growth of Yb:YLF may lead to reduced background absorption and nonradiative decay, offering an explanation for the outstanding laser cooling performance of this material. In contrast, fabrication of a laser cooling glass such as Yb:ZBLAN does not benefit from this purification step because all of the metal impurities that are present in the original glass melt will be incorporated into the final glass during melt quenching. The preparation of Yb:YLF capable of sub-100 K optical refrigeration will likely require a combination of purification of YF_3, LiF, and YbF_3 starting materials with crystal growth under carefully controlled conditions.

Yb:YLF crystals can be grown by the Czochralski [132–136] or the Bridgman–Stockbarger technique [116,136–138]. Use of this crystal for laser cooling applications requires starting materials of exceedingly high purity, as described above, which also aids in the growth of high-quality crystals. Abell *et al.* have shown that the often reported peritectic melting behavior of $YLiF_4$ is due to water and oxygen contaminations [139]. They achieved congruent but nonstoichiometric melting of $Y_{0.52}Li_{0.48}F_4$ provided that the starting materials were first treated in hot HF gas, the initial $YLiF_4$ product was zone-refined under argon, and the crystal was subsequently grown by the Czochralski technique under argon. The purity of argon was identified as a key factor, and passing the argon through a molecular sieve and over titanium heated to 700°C provided a sufficiently water- and oxygen-free atmosphere for zone-refinement and crystal growth. Such careful elimination of water and oxygen contaminants and tight process control are prerequisites for producing Yb:YLF crystals capable of sub-100 K optical refrigeration.

5. Summary

We reviewed recent advances in laser cooling of the Yb^{3+}:$YLiF_4$ crystal to cryogenic temperatures. A laser cooling model, aided by

detailed spectroscopic studies, predicts a global minimum achievable temperature (MAT_g) in Yb:YLF of 115 K when excited directly at the E4–E5 crystal-field resonance. The predicted MAT(λ) spectrum together with the MAT_g value at 1020 nm were verified in local cooling experiments. Results of bulk cooling of Yb:YLF to 155 K when pumped with a small detuning from the E4–E5 transition were discussed. Pumping exactly on resonance should yield temperatures approaching ~115 K for pumping levels below the saturation. As shown, a cooling power density of 3 W/cm^3 at 130 K should be possible in current-generation laser cooling crystals for pumping at saturation. Advanced material synthesis methods are needed to achieve laser cooling to temperatures below 100 K.

Acknowledgments

This work has been supported by the Air Force Office of Scientific Research (MURI program), DARPA (seedling), NASA, and the U.S. Department of Energy. D. V. Seletskiy acknowledges the support of a National Research Council Research Associateship Award at the Air Force Research Laboratory.

References and Notes

1. T. W. Hänsch and A. L. Schawlow, "Cooling of gases by laser radiation," Opt. Commun. **13**(1), 68–69 (1975).
2. S. Chu, C. Cohen-Tannoudji, and W. D. Philips, "For development of methods to cool and trap atoms with laser light," Nobel Prize in Physics (1997).
3. D. S. Jin and J. Ye, "Polar molecules in the quantum regime," Phys. Today **64**(5), 27 (2011).
4. S. Chu, L. Hollberg, J. E. Bjorkholm, A. Cable, and A. Ashkin, "Three-dimensional viscous confinement and cooling of atoms by resonance radiation pressure," Phys. Rev. Lett. **55**(1), 48–51 (1985).
5. E. A. Cornell, "Bose–Einstein condensation in a dilute gas; the first 70 years and some recent experiments," Nobel Prize in Physics, I (2001).
6. P. Pringsheim, "Zwei bemerkungen uber den unterschied von lumineszenz- und temperaturstrahlung," Z. Phys. **57**(11–12), 739–746 (1929).
7. L. Landau, "On the thermodynamics of photoluminescence," J. Phys. (Moscow) **10**, 503–506 (1946).
8. N. Djeu and W. T. Whitney, "Laser cooling by spontaneous anti-Stokes scattering," Phys. Rev. Lett. **46**(4), 236–239 (1981).
9. R. I. Epstein, M. I. Buchwald, B. C. Edwards, T. R. Gosnell, and C. E. Mungan, "Observation of laser-induced fluorescent cooling of a solid," Nature **377**(6549), 500–503 (1995).
10. J. L. Clark and G. Rumbles, "Laser cooling in the condensed phase by frequency up-conversion," Phys. Rev. Lett. **76**(12), 2037–2040 (1996).
11. R. Epstein and M. Sheik-Bahae, *Optical Refrigeration: Science and Applications of Laser Cooling of Solids*, 1st ed. (Wiley-VCH, 2009).
12. M. Sheik-Bahae and R. I. Epstein, "Optical refrigeration," Nat. Photonics **1**(12), 693–699 (2007).

13. M. Sheik-Bahae and R. I. Epstein, "Laser cooling of solids," Laser Photonics Rev. **3**(1–2), 67–84 (2009).
14. G. Nemova and R. Kashyap, "Laser cooling of solids," Rep. Prog. Phys. **73**(8), 086501 (2010).
15. S. V. Petrushkin and V. V. Samartsev, "Advances of laser refrigeration in solids," Laser Phys. **20**(1), 38–46 (2010).
16. D. V. Seletskiy, S. D. Melgaard, S. Bigotta, A. Di Lieto, M. Tonelli, and M. Sheik-Bahae, "Laser cooling of solids to cryogenic temperatures," Nat. Photonics **4**(3), 161–164 (2010).
17. M. Sheik-Bahae and R. I. Epstein, "Can laser light cool semiconductors," Phys. Rev. Lett. **92**(24), 247403 (2004).
18. P. Asbeck, "Self-absorption effects on the radiative lifetime in GaAs-GaAlAs double heterostructures," J. Appl. Phys. **48**(2), 820 (1977).
19. A. Kastler, "Some suggestions concerning the production and detection by optical means of inequalities in the populations of levels of spatial quantization in atoms. Application to the Stern and Gerlach and magnetic resonance experiments," J. Phys. Radium **11**, 11 (1950).
20. S. Yatsiv, "Anti-Stokes fluorescence as a cooling process," in *Advances in Quantum Electronics*, J. R. Singer, ed. (Columbia University, 1961).
21. T. Kushida and J. E. Geusic, "Optical refrigeration in Nd-doped yttrium aluminum garnet," Phys. Rev. Lett. **21**(16), 1172–1175 (1968).
22. C. E. Mungan, M. I. Buchwald, B. C. Edwards, R. I. Epstein, and T. R. Gosnell, "Laser cooling of a solid by 16 K starting from room temperature," Phys. Rev. Lett. **78**(6), 1030–1033 (1997).
23. X. Luo, M. D. Eisaman, and T. R. Gosnell, "Laser cooling of a solid by 21 K starting from room temperature," Opt. Lett. **23**(8), 639–641 (1998).
24. T. R. Gosnell, "Laser cooling of a solid by 65 K starting from room temperature," Opt. Lett. **24**(15), 1041–1043 (1999).
25. J. Thiede, J. Distel, S. R. Greenfield, and R. I. Epstein, "Cooling to 208 K by optical refrigeration," Appl. Phys. Lett. **86**(15), 154107 (2005).
26. B. C. Edwards, J. E. Anderson, R. I. Epstein, G. L. Mills, and A. J. Mord, "Demonstration of a solid-state optical cooler: an approach to cryogenic refrigeration," J. Appl. Phys. **86**(11), 6489 (1999).
27. A. Rayner, M. E. J. Friese, A. G. Truscott, N. R. Heckenberg, and H. Rubinsztein-Dunlop, "Laser cooling of a solid from ambient temperature," J. Mod. Opt. **48**, 103–114 (2001).
28. M. T. Murtagh, G. H. Sigel Jr., J. C. Fajardo, B. C. Edwards, and R. I. Epstein, "Laser-induced fluorescent cooling of rare-earth-doped fluoride glasses," J. Non-Cryst. Solids **253**(1–3), 50–57 (1999).
29. A. Rayner, N. R. Heckenberg, and H. Rubinsztein-Dunlop, "Condensed-phase optical refrigeration," J. Opt. Soc. Am. B **20**(5), 1037–1053 (2003).
30. B. Heeg, M. D. Stone, A. Khizhnyak, G. Rumbles, G. Mills, and P. A. DeBarber, "Experimental demonstration of intracavity solid-state laser cooling of Yb^{3+}:ZrF_4-BaF_2-LaF_3-AlF_3-NaF glass," Phys. Rev. A **70**(2), 021401 (2004).
31. D. V. Seletskiy, M. P. Hasselbeck, and M. Sheik-Bahae, "Resonant cavity-enhanced absorption for optical refrigeration," Appl. Phys. Lett. **96**(18), 181106 (2010).
32. W. M. Patterson, D. V. Seletskiy, M. Sheik-Bahae, R. I. Epstein, and M. P. Hehlen, "Measurement of solid-state optical refrigeration by two-band differential luminescence thermometry," J. Opt. Soc. Am. B **27**(3), 611–618 (2010).

33. J. R. Fernandez, "Origin of laser-induced internal cooling of Yb," Proc. SPIE **4645**, 135–147 (2002).
34. C. E. Mungan and T. R. Gosnell, "Laser cooling of solids," in *Advances in Atomic, Molecular, and Optical Physics*, Vol. 40, B. Bederson and H. Walther, ed. (Academic, 1999), pp. 161–228.
35. J. Fernández, A. Mendioroz, A. J. García, R. Balda, and J. L. Adam, "Anti-Stokes laser-induced internal cooling of Yb^{3+}-doped glasses," Phys. Rev. B **62**(5), 3213–3217 (2000).
36. J. Fernández, A. Mendioroz, A. J. García, R. Balda, J. L. Adam, and M. A. Arriandiaga, "On the origin of anti-Stokes laser-induced cooling of Yb^{3+}-doped glass," Opt. Mater. **16**(1–2), 173–179 (2001).
37. S. R. Bowman and C. E. Mungan, "New materials for optical cooling," Appl. Phys. B **71**(6), 807–811 (2000).
38. R. I. Epstein, J. J. Brown, B. C. Edwards, and A. Gibbs, "Measurements of optical refrigeration in ytterbium-doped crystals," J. Appl. Phys. **90**(9), 4815 (2001).
39. A. Mendioroz, J. Fernández, M. Voda, M. Al-Saleh, R. Balda, and A. J. García-Adeva, "Anti-Stokes laser cooling in Yb^{3+}-doped KPb_2Cl_5 crystal," Opt. Lett. **27**(17), 1525–1527 (2002).
40. S. Bigotta, D. Parisi, L. Bonelli, A. Toncelli, M. Tonelli, and A. Di Lieto, "Spectroscopic and laser cooling results on Yb^{3+}-doped BaY_2F_8 single crystal," J. Appl. Phys. **100**(1), 013109 (2006).
41. S. Bigotta, D. Parisi, L. Bonelli, A. Toncelli, A. D. Lieto, and M. Tonelli, "Laser cooling of Yb^{3+}-doped BaY_2F_8 single crystal," Opt. Mater. **28**(11), 1321–1324 (2006).
42. S. Bigotta, A. Di Lieto, D. Parisi, A. Toncelli, and M. Tonelli, "Single fluoride crystals as materials for laser cooling applications," Proc. SPIE **6461**, 64610E (2007).
43. S. Bigotta, "Laser cooling of solids: new results with single fluoride crystals," Nuovo Cimento B Ser. **122**, 685694 (2007).
44. D. Seletskiy, M. P. Hasselbeck, M. Sheik-Bahae, R. I. Epstein, S. Bigotta, and M. Tonelli, "Cooling of Yb:YLF using cavity enhanced resonant absorption," Proc. SPIE **6907**, 69070B (2008).
45. J. V. Guiheen, C. D. Haines, G. H. Sigel, R. I. Epstein, J. Thiede, and W. M. Patterson, "Yb^{3+} and Tm^{3+}-doped fluoroaluminate classes for anti-Stokes cooling," Phys. Chem. Glasses Eur. J. Glass Sci. Technol. Part B **47**, 167–176 (2006).
46. C. W. Hoyt, M. Sheik-Bahae, R. I. Epstein, B. C. Edwards, and J. E. Anderson, "Observation of anti-Stokes fluorescence cooling in thulium-doped glass," Phys. Rev. Lett. **85**(17), 3600–3603 (2000).
47. C. W. Hoyt, M. P. Hasselbeck, M. Sheik-Bahae, R. I. Epstein, S. Greenfield, J. Thiede, J. Distel, and J. Valencia, "Advances in laser cooling of thulium-doped glass," J. Opt. Soc. Am. B **20**(5), 1066–1074 (2003).
48. W. Patterson, S. Bigotta, M. Sheik-Bahae, D. Parisi, M. Tonelli, and R. Epstein, "Anti-Stokes luminescence cooling of Tm^{3+} doped BaY_2F_8," Opt. Express **16**(3), 1704–1710 (2008).
49. J. Fernandez, A. J. Garcia-Adeva, and R. Balda, "Anti-stokes laser cooling in bulk erbium-doped materials," Phys. Rev. Lett. **97**(3), 033001 (2006).
50. N. J. Condon, S. R. Bowman, S. P. O'Connor, R. S. Quimby, and C. E. Mungan, "Optical cooling in Er^{3+}:KPb_2Cl_5," Opt. Express **17**(7), 5466–5472 (2009).

51. A. N. Oraevsky, "Cooling of semiconductors by laser radiation," J. Russ. Laser Res. **17**(5), 471–479 (1996).
52. L. Rivlin and A. Zadernovsky, "Laser cooling of semiconductors," Opt. Commun. **139**(4–6), 219–222 (1997).
53. T. Apostolova, D. Huang, P. M. Alsing, and D. A. Cardimona, "Comparison of laser cooling of the lattice of wide-band-gap semiconductors using nonlinear or linear optical excitations," Phys. Rev. A **71**(1), 013810 (2005).
54. G. Rupper, N. H. Kwong, and R. Binder, "Large excitonic enhancement of optical refrigeration in semiconductors," Phys. Rev. Lett. **97**(11), 117401 (2006).
55. J. Li, "Laser cooling of semiconductor quantum wells: theoretical framework and strategy for deep optical refrigeration by luminescence upconversion," Phys. Rev. B **75**(15), 155315 (2007).
56. J. B. Khurgin, "Role of bandtail states in laser cooling of semiconductors," Phys. Rev. B **77**(23), 235206 (2008).
57. G. Rupper, N. H. Kwong, and R. Binder, "Optical refrigeration of GaAs: theoretical study," Phys. Rev. B **76**(24), 245203 (2007).
58. J. B. Khurgin, "Surface plasmon-assisted laser cooling of solids," Phys. Rev. Lett. **98**(17), 177401 (2007).
59. D. Huang and P. M. Alsing, "Many-body effects on optical carrier cooling in intrinsic semiconductors at low lattice temperatures," Phys. Rev. B **78**(3), 035206 (2008).
60. P. G. Eliseev, "Anti-Stokes luminescence in heavily doped semiconductors as a mechanism of laser cooling," Opto-Electron. Rev. **16**, 199–207 (2008).
61. G. Rupper, N. H. Kwong, R. Binder, C.-Y. Li, and M. Sheik-Bahae, "Effect of n–p–n heterostructures on interface recombination and semiconductor laser cooling," J. Appl. Phys. **108**(11), 113118 (2010).
62. H. Gauck, T. H. Gfroerer, M. J. Renn, E. A. Cornell, and K. A. Bertness, "External radiative quantum efficiency of 96% from a GaAs/GaInP heterostructure," Appl. Phys., A Mater. Sci. Process. **64**(2), 143–147 (1997).
63. E. Finkeißen, M. Potemski, P. Wyder, L. Viña, and G. Weimann, "Cooling of a semiconductor by luminescence up-conversion," Appl. Phys. Lett. **75**(9), 1258 (1999).
64. T. H. Gfroerer, E. A. Cornell, and M. W. Wanlass, "Efficient directional spontaneous emission from an InGaAs/InP heterostructure with an integral parabolic reflector," J. Appl. Phys. **84**(9), 5360 (1998).
65. B. Imangholi, M. P. Hasselbeck, M. Sheik-Bahae, R. I. Epstein, and S. Kurtz, "Effects of epitaxial lift-off on interface recombination and laser cooling in GaInP/GaAs heterostructures," Appl. Phys. Lett. **86**(8), 081104 (2005).
66. B. Imangholi, "Investigation of laser cooling in semiconductors," Ph.D. dissertation (University of Mexico, 2006).
67. S. Eshlaghi, W. Worthoff, A. D. Wieck, and D. Suter, "Luminescence upconversion in GaAs quantum wells," Phys. Rev. B **77**(24), 245317 (2008).
68. M. P. Hasselbeck, M. Sheik-Bahae, and R. I. Epstein, "Effect of high carrier density on luminescence thermometry in semiconductors," Proc. SPIE **6461**, 646107 (2007).

69. C. Wang, C.-Y. Li, M. P. Hasselbeck, B. Imangholi, and M. Sheik-Bahae, "Precision, all-optical measurement of external quantum efficiency in semiconductors," J. Appl. Phys. **109**(9), 093108 (2011).
70. B. C. Edwards, M. I. Buchwald, and R. I. Epstein, "Development of the Los Alamos solid-state optical refrigerator," Rev. Sci. Instrum. **69**(5), 2050 (1998).
71. S. R. Bowman, "Lasers without internal heat generation," IEEE J. Quantum Electron. **35**(1), 115–122 (1999).
72. S. R. Bowman, S. P. O'Connor, S. Biswal, N. J. Condon, and A. Rosenberg, "Minimizing heat generation in solid-state lasers," IEEE J. Quantum Electron. **46**(7), 1076–1085 (2010).
73. A. Sugiyama, M. Katsurayama, Y. Anzai, and T. Tsuboi, "Spectroscopic properties of Yb doped YLF grown by a vertical Bridgman method," J. Alloy. Comp. **408–412**, 780–783 (2006).
74. D. V. Seletskiy, S. D. Melgaard, A. Di Lieto, M. Tonelli, and M. Sheik-Bahae, "Laser cooling of a semiconductor load to 165 K," Opt. Express **18**(17), 18061–18066 (2010).
75. D. V. Seletskiy, R. I. Epstein, and M. Sheik-Bahae, "Progress toward sub-100 Kelvin operation of an optical cryocooler," Proc. SPIE **7951**, 795103 (2011).
76. U. Vogl and M. Weitz, "Laser cooling by collisional redistribution of radiation," Nature **461**(7260), 70–73 (2009).
77. M. Sheik-Bahae and D. Seletskiy, "Laser cooling: chilling dense atomic gases," Nat. Photonics **3**(12), 680–681 (2009).
78. A. Saß, U. Vogl, and M. Weitz, "Laser cooling of a potassium–argon gas mixture using collisional redistribution of radiation," Appl. Phys. B **102**(3), 503–507 (2011).
79. G. Bahl, M. Tomes, F. Marquardt, and T. Carmon, "Observation of spontaneous Brillouin cooling," Nat. Phys. 8, 203–207 (2012).
80. N. Vermeulen, C. Debaes, P. Muys, and H. Thienpont, "Mitigating heat dissipation in Raman lasers using coherent anti-stokes Raman scattering," Phys. Rev. Lett. **99**(9), 093903 (2007).
81. S. C. Rand, "Laser cooling of solids by stimulated Raman scattering and fluorescence," Proc. SPIE **8275**, 827509 (2012).
82. S. V. Petrushkin and V. V. Samartsev, "Superradiance regime of laser cooling of crystals and glasses doped with rare-earth ion," Laser Phys. **11**, 948–956 (2001).
83. G. Nemova and R. Kashyap, "Alternative technique for laser cooling with superradiance," Phys. Rev. A **83**(1), 013404 (2011).
84. S. N. Andrianov and V. V. Samartsev, "Solid state lasers with internal laser refrigeration effect," Proc. SPIE **4605**, 208–213 (2001).
85. G. Nemova and R. Kashyap, "Fiber amplifier with integrated optical cooler," J. Opt. Soc. Am. B **26**(12), 2237–2241 (2009).
86. G. Nemova and R. Kashyap, "Raman fiber amplifier with integrated cooler," J. Lightwave Technol. **27**(24), 5597–5601 (2009).
87. G. Nemova and R. Kashyap, "High-power fiber lasers with integrated rare-earth optical cooler," Proc. SPIE **7614**, 761406(2010).
88. C. H. Metzger and K. Karrai, "Cavity cooling of a microlever," Nature **432**(7020), 1002–1005 (2004).
89. J. D. Teufel, T. Donner, D. Li, J. W. Harlow, M. S. Allman, K. Cicak, A. J. Sirois, J. D. Whittaker, K. W. Lehnert, and R. W. Simmonds,

"Sideband cooling of micromechanical motion to the quantum ground state," Nature **475**(7356), 359–363 (2011).
90. S. N. Andrianov and V. V. Samartsev, "Laser cooling of impurity crystals," Quantum Electron. **31**(3), 247–251 (2001).
91. D. Huang, T. Apostolova, P. M. Alsing, and D. A. Cardimona, "Theoretical study of laser cooling of a semiconductor," Phys. Rev. B **70**(3), 033203 (2004).
92. J. Kim and M. Kaviany, "Ab initio calculations of f-orbital electron–phonon interaction in laser cooling," Phys. Rev. B **79**(5), 054103 (2009).
93. M. P. Hehlen, R. I. Epstein, and H. Inoue, "Model of laser cooling in the Yb^{3+}-doped fluorozirconate glass ZBLAN," Phys. Rev. B **75**(14), 144302 (2007).
94. N. Coluccelli, G. Galzerano, L. Bonelli, A. Di Lieto, M. Tonelli, and P. Laporta, "Diode-pumped passively mode-locked Yb:YLF laser," Opt. Express **16**(5), 2922–2927 (2008).
95. D. V. Seletskiy, S. D. Melgaard, R. I. Epstein, A. Di Lieto, M. Tonelli, and M. Sheik-Bahae, "Precise determination of minimum achievable temperature for solid-state optical refrigeration," J. Lumin. (to be published); corrected proof, http://dx.doi.org/10.1016/j.jlumin.2011.09.045.
96. D. V. Seletskiy, S. D. Melgaard, R. I. Epstein, A. Di Lieto, M. Tonelli, and M. Sheik-Bahae, "Local laser cooling of Yb:YLF to 110 K," Opt. Express **19**(19), 18229–18236 (2011).
97. D. E. McCumber, "Einstein relations connecting broadband emission and absorption spectra," Phys. Rev. **136**(4A), A954–A957 (1964).
98. G. Lei, J. E. Anderson, M. I. Buchwald, B. C. Edwards, R. I. Epstein, M. T. Murtagh, and G. H. Sigel, "Spectroscopic evaluation of Yb^{3+}-doped glasses for optical refrigeration," IEEE J. Quantum Electron. **34**(10), 1839–1845 (1998).
99. G. Lei, J. Anderson, M. Buchwald, B. Edwards, and R. Epstein, "Determination of spectral linewidths by Voigt profiles in Yb^{3+}-doped fluorozirconate glasses," Phys. Rev. B **57**(13), 7673–7678 (1998).
100. A. Bensalah, Y. Guyot, A. Brenier, H. Sato, T. Fukuda, and G. Boulon, "Spectroscopic properties of Yb^{3+}:$LuLiF_4$ crystal grown by the Czochralski method for laser applications and evaluation of quenching processes: a comparison with Yb^{3+}: $YLiF_4$," J. Alloy. Comp. **380**(1–2), 15–26 (2004).
101. A. Yariv, "Universal relations for coupling of optical power between microresonators and dielectric waveguides," Electron. Lett. **36**(4), 321–322 (2000).
102. A. E. Siegman, *Lasers* (University Science Books, 1986).
103. K. Kishino, M. S. Unlu, J.-I. Chyi, J. Reed, L. Arsenault, and H. Morkoc, "Resonant cavity-enhanced (RCE) photodetectors," IEEE J. Quantum Electron. **27**(8), 2025–2034 (1991).
104. Y. D. Chong, L. Ge, H. Cao, and A. D. Stone, "Coherent perfect absorbers: time-reversed lasers," Phys. Rev. Lett. **105**(5), 053901 (2010).
105. C. Hoyt, "Laser cooling in thulium-doped solids," Ph.D. dissertation (University of New Mexico, 2003).
106. A. R. Albrecht, D. V. Seletskiy, J. G. Cederberg, A. Di Lieto, M. Tonelli, J. Moloney, G. Balakrishnan, and M. Sheik-Bahae, "Intracavity laser cooling using a VECSEL," Proc. SPIE **8275**, 827505 (2012).

107. B. Imangholi, M. Hasselbeck, D. Bender, C. Wang, M. Sheik-Bahae, R. Epstein, and S. Kurtz, "Differential luminescence thermometry in semiconductor laser cooling," Proc. SPIE **6115**, 61151C (2006).
108. B. Heeg, G. Rumbles, A. Khizhnyak, and P. A. DeBarber, "Comparative intra- versus extra-cavity laser cooling efficiencies," J. Appl. Phys. **91**(5), 3356–3362 (2002).
109. G. Mills and A. Mord, "Performance modeling of optical refrigerators," Cryogenics **46**(2–3), 176–182 (2006).
110. J. Parker, D. Mar, S. Von der Porten, J. Hankinson, K. Byram, C. Lee, M. K. Mayeda, R. Haskell, Q. Yang, S. Greenfield, and R. Epstein, "Thermal links for the implementation of an optical refrigerator," J. Appl. Phys. **105**(1), 013116 (2009).
111. M. P. Hehlen, "Design and fabrication of rare-earth-doped laser cooling materials," in *Optical Refrigeration: Science and Applications of Laser Cooling of Solids*, R. Epstein and M. Sheik-Bahae, ed. (Wiley-VCH Verlag GmbH & Co, KGaA, 2009), pp. 33–74.
112. J. M. F. van Dijk, "On the nonradiative and radiative decay rates and a modified exponential energy gap law for 4f–4f transitions in rare-earth ions," J. Chem. Phys. **78**(9), 5317 (1983).
113. L. A. Riseberg and H. W. Moos, "Multiphonon orbit-lattice relaxation of excited states of rare-earth ions in crystals," Phys. Rev. **174**(2), 429–438 (1968).
114. P. C. Schultz, L. J. B. Vacha, C. T. Moynihan, B. B. Harbison, K. Cadien, and R. Mossadegh, "Hermetic coatings for bulk fluoride glasses and fibers," Mater. Sci. Forum **19–20**, 343–352 (1987).
115. P. W. France, S. F. Carter, J. R. Williams, K. J. Beales, and J. M. Parker, "OH^- absorption in fluoride glass infra-red fibres," Electron. Lett. **20**(14), 607–608 (1984).
116. R. Burkhalter, I. Dohnke, and J. Hulliger, "Growing of bulk crystals and structuring waveguides of fluoride materials for laser applications," Prog. Cryst. Growth Charact. Mater. **42**(1–2), 1–64 (2001).
117. S. W. Kwon, E. H. Kim, B. G. Ahn, J. H. Yoo, and H. G. Ahn, "Fluorination of metals and metal oxides by gas-solid reaction," J. Ind. Eng. Chem. **8**, 477 (2002).
118. K. W. Krämer, D. Biner, G. Frei, H. U. Güdel, M. P. Hehlen, and S. R. Lüthi, "Hexagonal sodium yttrium fluoride based green and blue emitting upconversion phosphors," Chem. Mater. **16**(7), 1244–1251 (2004).
119. J. Ferguson, E. R. Krausz, and H. J. Guggenheim, "MCD spectroscopy of transition metal ions in fluoride crystals," Mol. Phys. **29**(6), 1785–1796 (1975).
120. W. Gehlhoff and W. Ulrici, "Transition metal ions in crystals with the fluorite structure," Phys. Status Solidi, B Basic Res. **102**(1), 11–59 (1980).
121. A. A. Kaminskii, *Laser Crystals: Their Physics and Properties*, 1st ed. (Springer, 1981).
122. A. Illarramendi, J. Fernández, and R. Balda, "Fano antiresonance of Cr^{3+} absorption spectra in flouride glasses," J. Lumin. **53**(1–6), 461–464 (1992).
123. C. R. Mendonça, B. J. Costa, Y. Messaddeq, and S. C. Zilio, "Optical properties of chromium-doped fluoroindate glasses," Phys. Rev. B **56**(5), 2483–2487 (1997).

124. L. Seijo, Z. Barandiarán, and D. S. McClure, "Ab initio model potential embedded cluster calculation of the absorption spectrum of Cs_2GeF_6:Mn^{4+}. Large discrepancies between theory and experiment," Int. J. Quantum Chem. **80**, 623–635 (2000).
125. I. Hernández, F. Rodríguez, and A. Tressaud, "Optical properties of the $(CrF_6)^{3-}$ complex in A_2BMF_6: Cr^{3+} elpasolite crystals: variation with M–F bond distance and hydrostatic pressure," Inorg. Chem. **47**(22), 10288–10298 (2008).
126. U. Brauch and U. Dürr, "Vibronic laser action of V^{2+}:$CsCaF_3$," Opt. Commun. **55**(1), 35–40 (1985).
127. M. J. Elejalde, R. Balda, and J. Fernández, "Optical properties of Ni^{2+} in fluoride investigated by time-resolved spectroscopy," J. Phys. IV **04**(C4), C4-411 (1994).
128. P. W. France, S. F. Carter, and J. M. Parker, "Oxidation states of 3d transition metals in ZrF_4 glasses," Phys. Chem. Glasses **27**, 32 (1986).
129. K. Tanimura, W. A. Sibley, and L. G. DeShazer, "Optical properties of Cu^+ ions in $RbMgF_3$ crystals," Phys. Rev. B Condens. Matter **31**(6), 3980–3987 (1985).
130. S. Bigotta, *Energy Transfer and Cooling Processes in Rare-earth Doped Insulating Crystals* (Universita di Pisa, 2006).
131. W. M. Patterson, P. C. Stark, T. M. Yoshida, M. Sheik-Bahae, and M. P. Hehlen, "Preparation and characterization of high-purity metal fluorides for photonic applications," J. Am. Ceram. Soc. **94**(9), 2896–2901 (2011).
132. D. Gabbe and A. L. Harmer, "Scheelite structure fluorides: the growth of pure and rare earth doped $LiYF_4$," J. Cryst. Growth **3–4**, 544 (1968).
133. I. A. Ivanova, A. M. Morozov, M. A. Petrova, I. G. Podkolzina, and P. P. Feotilov, "Growth of binary lithium-rare earth metal fluoride monocrystals and their properties," Izv. Akad. Nauk SSSR Neorg. Mater. **11**, 2175–2179 (1975).
134. R. Uhrin, R. F. Belt, and V. Rosati, "Preparation and crystal growth of lithium yttrium fluoride for laser applications," J. Cryst. Growth **38**(1), 38–44 (1977).
135. I. M. Ranieri, S. L. Baldochi, A. M. E. Santo, L. Gomes, L. C. Courrol, L. V. G. Tarelho, W. de Rossi, J. R. Berretta, F. E. Costa, G. E. C. Nogueira, N. U. Wetter, D. M. Zezell, N. D. Vieira Jr., and S. P. Morato, "Growth of $LiYF_4$ crystals doped with holmium, erbium and thulium," J. Cryst. Growth **166**(1–4), 423–428 (1996).
136. P. J. Walker, "Melt growth of rare-earth binary and complex halides," Prog. Cryst. Growth Characteriz. **3**(2–3), 103–119 (1980).
137. W. A. Shand, "Single crystal growth and some properties of $LiYF_4$," J. Cryst. Growth **5**(2), 143–146 (1969).
138. D. A. Jones, B. Cockayne, R. A. Clay, and P. A. Forrester, "Stockbarger crystal growth, optical assessment and laser performance of holmium-doped yttrium erbium lithium fluoride," J. Cryst. Growth **30**(1), 21–26 (1975).
139. J. S. Abell, I. R. Harris, B. Cockayne, and J. G. Plant, "A DTA study of zone-refined $LiRF_4$ ($R = Y, Er$)," J. Mater. Sci. **11**(10), 1807–1816 (1976).

Denis V. Seletskiy is a National Research Council Postdoctoral Associate at the Air Force Research Laboratory in New Mexico. He received his Ph.D. with distinction in Optical Science and Engineering from the University of New Mexico in 2010. His research interests include solid-state laser cooling, nonlinear optics, and ultrafast phenomena focusing on terahertz spectroscopy of condensed matter.

Markus P. Hehlen is a Staff Scientist and Team Leader at Los Alamos National Laboratory (LANL) and Adjunct Research Associate Professor at the University of New Mexico. He received his Ph.D. in Inorganic Chemistry from the University of Bern, Switzerland, and conducted his postdoctoral work at LANL and the University of Michigan. He was Senior Research Scientist and Project Manager at Gemfire Corporation, where he developed phosphors and compact fiber-optic amplifiers. He rejoined LANL in 2003 and currently works on the development of new optical materials and optoelectronic devices for defense, homeland security, and threat reduction applications. He is a Founding Associate Editor of *Optical Materials Express*.

Richard I. Epstein is The CEO of ThermoDynamic Films LLC in New Mexico and an adjunct professor at the University of New Mexico. He was an undergraduate in Engineering Physics at Cornell University and received his Ph.D. in Applied Physics from Stanford University. He did research at the University of Texas at Austin, Harvard University and Nordita in Copenhagen, and then joined Los Alamos National Laboratory where he was a Laboratory Fellow and led the effort in optical refrigeration. He has published over 160 papers in theoretical astrophysics, satellite instrumentation, and applied physics. He is a fellow of the Optical Society of America.

Mansoor Sheik-Bahae is a professor of Physics and Astronomy and the chair of Optical Science and Engineering at the University of New Mexico (UNM), Albuquerque, New Mexico (USA). He graduated from the State University of New York (Buffalo), and subsequently spent seven years as a research scientist at CREOL—University of Central Florida before joining UNM in 1994, where he currently heads the Consortium for Laser Cooling of Solids. Professor Sheik-Bahae has authored more than 200 scientific papers in nonlinear optics, ultrafast phenomena, and solid-state laser cooling, with more than 7000 citations to his work. He is a fellow of Optical Society of America and the recipient of society's R. W. Wood prize in 2012.